sustainability

MDPI

Article

Analysis and Optimization of Entry Stability in Underground Longwall Mining

Yubing Gao [1,2], Dongqiao Liu [1,2], Xingyu Zhang [1,2] and Manchao He [1,*]

[1] State Key Laboratory of Geomechanics & Deep Underground Engineering, China University of Mining & Technology, Beijing 100083, China; yubing.gao@yahoo.com (Y.G.); liudq1012@126.com (D.L.); xuanlanwu@163.com (X.Z.)

[2] School of Mechanics and Civil Engineering, China University of Mining & Technology, Beijing 100083, China

* Correspondence: manchaohecumt@163.com

Received: 1 October 2017; Accepted: 10 November 2017; Published: 12 November 2017

Abstract: For sustainable utilization of limited coal resources, it is important to increase the coal recovery rate and reduce mine accidents, especially those occurring in the entry (gateroad). Entry stabilities are vital for ventilation, transportation and other essential services in underground coal mining. In the present study, a finite difference model was built to investigate stress evolutions around the entry, and true triaxial tests were carried out at the laboratory to explore entry wall stabilities under different mining conditions. The modeling and experimental results indicated that a wide coal pillar was favorable for entry stabilities, but oversize pillars caused a serious waste of coal resources. As the width of the entry wall decreased, the integrated vertical stress, induced by two adjacent mining panels, coupled with each other and experienced an increase on the entry wall, which inevitably weakened the stability of the entry. Therefore, mining with coal pillars always involves a tradeoff between economy and safety. To address this problem, an innovative non-pillar mining technique by optimizing the entry surrounding structures was proposed. Numerical simulation showed that the deformation of the entry roof decreased by approximately 66% after adopting the new approach, compared with that using the conventional mining method. Field monitoring indicated that the stress condition of the entry was significantly improved and the average roof pressure decreased by appropriately 60.33% after adopting the new technique. This work provides an economical and effective approach to achieve sustainable exploitation of underground coal resources.

Keywords: sustainable exploitation; coal resources; longwall mining; entry stability

1. Introduction

Coal is among the most important foundational energies, accounting for approximately 30% of the total energy consumption around the world [1,2]. For sustainable utilization of limited coal resources, it is imperative to increase the coal recovery rate and improve mining safety. Failure or collapse of the entry, which can lead to human loss or interruption of mining, is a common accident in the mine. Entry stabilities are related to the surrounding stress conditions. Mahdi et al. [3] carried out a numerical investigation on how longwall mining affected the stress state in the border area and how the stress changes would affect future mining. They found that the pillar stress fluctuated up and down during mining, and the failure zone of a pillar was approximately 12 m from the entry rib to the wall center. Suchowerska et al. [4] investigated some variables that affected stress redistributions. They found that the abutment angle of the pillar loading has a greater effect than other factors such as the overburden depth. Basarir et al. [5] predicted the stresses around the entry using empirical and numerical analysis of different mining methods (the fully mechanized traditional longwall and longwall top coal caving methods). Such issues have also been addressed in the literature [6–10]. These studies showed that the stress redistribution around the entry is associated with many factors such as geologic setting,

working face layout and mining disturbances. Certainly, the entry surroundings, especially the coal pillar between two adjacent mining panels, has an important influence on stress distributions around the entry.

In terms of entry wall (coal pillar) stabilities, most previous studies were conducted through theoretical analysis and numerical simulation. For example, Gao [11] evaluated pillar stabilities using the limiting-equilibrium theory. In his study, the coal pillar was divided into three zones: the loose zone, plastic zone and elastic zone. Wang et al. [12] proposed an approach to simulate the static and dynamic behaviors of the coal pillar. They concluded that the width-to-height (W/H) ratio of the coal pillar was important in affecting entry wall stabilities. Bieniawski, Reed and other researchers [13–15] developed different methods to design and optimize the pillar size. Presently, gob-side entry retaining by filling artificial materials is a frequently used non-pillar mining method to optimize sustainable mining. In this method, the former entry is artificially retained as the tailgate for the next mining panel by using pigsties, paste-like backfill material, high-water packing material, and other fill materials. In this mining pattern, non-pillar is left after mining. However, excessive consumption of filling materials and high stress concentration on the filling materials set limits on the popularity of this method applied in complicated geological conditions, such as thick coal seams. Therefore, it is necessary to find a more effective and economical method to improve mining sustainability and safety.

Previous studies reveal that the entry stability is primarily determined by its surrounding stresses [16–18]. Considering this, we proposed a stress optimization method that aims to increase the coal recovery rate and improve entry stabilities. First, the stability of the entry wall in conventional mining patterns was systematically studied using numerical modeling, laboratory test and theoretical analysis. Subsequently, a novel roof addressing technique was proposed and tested in the field. The applicative effects indicate that the proposed approach is effective and has broad application prospects in sustainable mining of underground coal resources.

2. Analysis of the Entry Stability in Conventional Mining Patterns

Technological advances in mining mechanization over the past decades have enabled longwall mining to supersede room and pillar mining in terms of both safety and production levels [19]. The dimensional design of the chain pillar between two mining panels is one of the main focus points in longwall mining. Entry wall stabilities to a great extent determine entry stabilities, especially in a high-stress entry. To explore the vulnerable surroundings of the entry and the reason that causes the entry to be unstable, numerical simulation, laboratory test and theoretical analysis were conducted, respectively. Since the width of the coal pillar is an important factor that influences stress distributions and entry stability, several scenarios that emphasizes the pillar width were performed. Distribution laws of the vertical stress around the entry were studied using numerical simulation, and failure states of the coal pillar were investigated using laboratory tests. Based on the obtained results, we then proposed pertinent strategies to address the instability problem of the entry.

2.1. Numerical Analysis of the Entry Wall Stability

2.1.1. Study Site

The Ningtiaota coal mine is located in Shanxi province, China. This mine produces approximately 20 million tons of coal annually. The selected panels are approximately 200~300 m wide and 3000 m long, with a dip angle of less than 2°. The mean thickness of the coal seam is 4.0 m, with an average overburden varying from 80 to 160 m. Figure 1 shows the mine location and column map of the stratum. The roof strata are mainly composed of hard sandstones, and the floor strata consist of siltstone (8.1 m) and fine-grain sandstone (12.3 m). Full-seam, comprehensive mechanized and retreating mining methods were used in the panels, and a spontaneous caving method was used to treat the gob roof during the mining process.

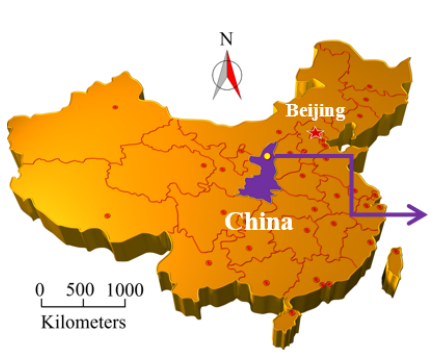

Columnar	Thickness (m)	Lithology	Remarks
	14.6	Medium-grain sandstone	Main roof
	8.40	Quartz sandstone	
	4.40	Siltstone	Immediate roof
	4.20	Coal	Coal seam 2-2
	8.10	Siltstone	Immediate floor
	12.3	Fine-grained sandstone	Main floor

Figure 1. Location of the mine and lithology of the rock layers.

2.1.2. Numerical Model

To investigate evolution laws of the vertical stress on the entry wall under different mining conditions, a 3D numerical model was developed using the finite difference method, as illustrated in Figure 2. The dimensions of the model were a length of 300 m, width of 200 m, and height of 150 m, based on the geological column. In this study, the excavation was performed by changing the mechanical properties of the coal seam in the caved area to a very soft elastic material, in which case, the bearing capacities of the caved rock could be fully considered. This analogy method of the excavation process has also been used by other researchers [20,21].

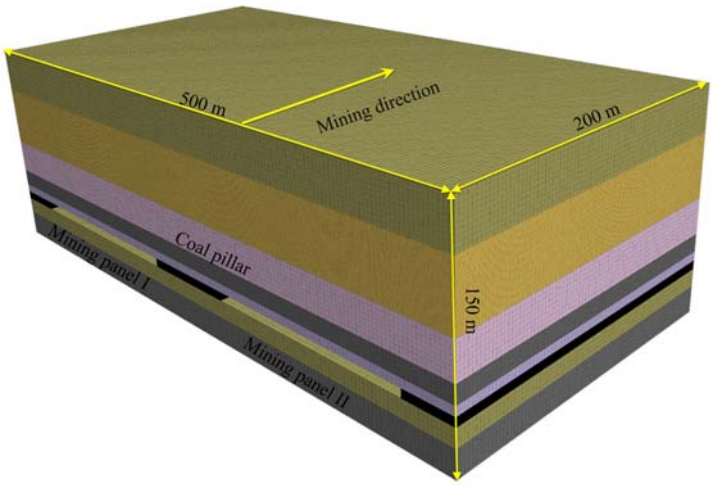

Figure 2. Schematic diagram of the numerical model.

In terms of the boundary constraints, the left and right borders restrict the horizontal displacement, and the lower bounder restricts the vertical displacement, respectively. The minimum horizontal stress-to-vertical stress ratio is kept as 0.8 according to the in-situ stresses of No. 2-2 coal seam. The constitutive equation adopted in this model is Mohr–Coulomb criterion, which is a mathematical model describing the response of brittle materials to shear stress as well as normal stress.

The properties of real rock masses in the field are usually different from those tested at the laboratory [22]. The elastic modulus, cohesion and tensile strength results are generally 0.1~0.25 of the laboratory testing results. The Poisson ratios are approximately 1.2~1.4 of the laboratory testing results. On the basis of the laboratory test results of the mechanical properties of the rock samples, the final property parameters of the rock strata in the numerical model are presented in Table 1.

Table 1. Mechanical parameters of the rock strata.

Rock Strata	Density (kg/m^3)	Elasticity Modulus (GPa)	Friction Angle (deg)	Cohesion (MPa)	Tensile Strength (MPa)
Overlying strata	2500	15.2	30	1.8	0.7
Fine sandstone	2650	19.6	32	2.3	1.2
Medium sandstone	2600	13.5	34	2.4	1.4
Quartz sandstone	2780	21.1	38	3.2	1.6
Siltstone	2550	16.5	30	2.1	0.9
No. 2-2 coal seam	1250	4.3	19	0.9	0.4
Siltstone	2550	13.9	26	3.0	1.2
Fine sandstone	2650	18.8	33	3.1	1.5

2.1.3. Evolution Laws of the Vertical Stress on the Entry Wall

In the numerical modeling, plane I and plane I were successively exploited to illustrate and analyze the recorded stress on the entry wall. The widths of the entry wall between planes I and II were 80 m, 50 m, 30 m, 15 m, 8 m and 5 m, respectively, which can be used to represent different mining patterns. The contour maps of the vertical stress are presented in Figure 3.

According to the simulation results, the following can be concluded:

(1). In terms of stress migration, the stress peaks moved closer to each other as the pillar width decreased. The macroscopic shape of the vertical stress was double-arched when the pillar widths were large (80 m, 50 m and 30 m). Gradually, the double-arched shape of the stress evolved into a single-arched shape (15 m, 8 m and 5 m), and the integrated peak stress increased as well. In fact, the vertical stress on the pillar was induced in two stages. In the first stage, the stress was induced by the production of the present panel (panel I). After the surrounding rocks had stabilized, the mining-induced stress gradually reached equilibrium and remained constant. Subsequently, as panel II was mined, and an additional stress was then superimposed on the existing stress. Finally, the vertical stress achieved equilibrium on the entry wall.

(2). In terms of the stress magnitudes, the position of the stress peak was in front of the panel. When the pillar width was more than 50 m, two stress peaks caused by panel I and II were distributed near the pillar sides. As the pillar width decreased, the central stress increased on the pillar, whereas the peak value remained unchanged (approximately 21.8 MPa). When the pillar widths were from 50 m to 30 m, there were also two stress peaks distributed on the two sides. However, the peak values increased quickly with decreasing pillar width. When the pillar width was less than 15 m, there was only one stress peak indicated macroscopically. The maximum vertical stress reached 27.8 MPa when the pillar width was 15 m. Interestingly, as the pillar width continued to decrease to 5 m, the peak stress decreased, as shown in Figure 3f. In a narrow pillar, there would be more mining-induced fractures distributed in the coal body. Essentially, the entry wall had been damaged. These fractures provided voids for the stress to release, causing the vertical stress to decrease.

As seen in the simulation results, there were always concentrated stresses distributed on the entry wall, regardless of the pillar size. Specifically, when the pillar was wide, the concentrated stress was relatively small. As the pillar width decreased, the overall vertical stress increased. When the pillar was too narrow to bear the concentrated stress, the entry wall coal was damaged. Accordingly, we can conclude that the concentrated stress was the main reason accounting for entry instabilities.

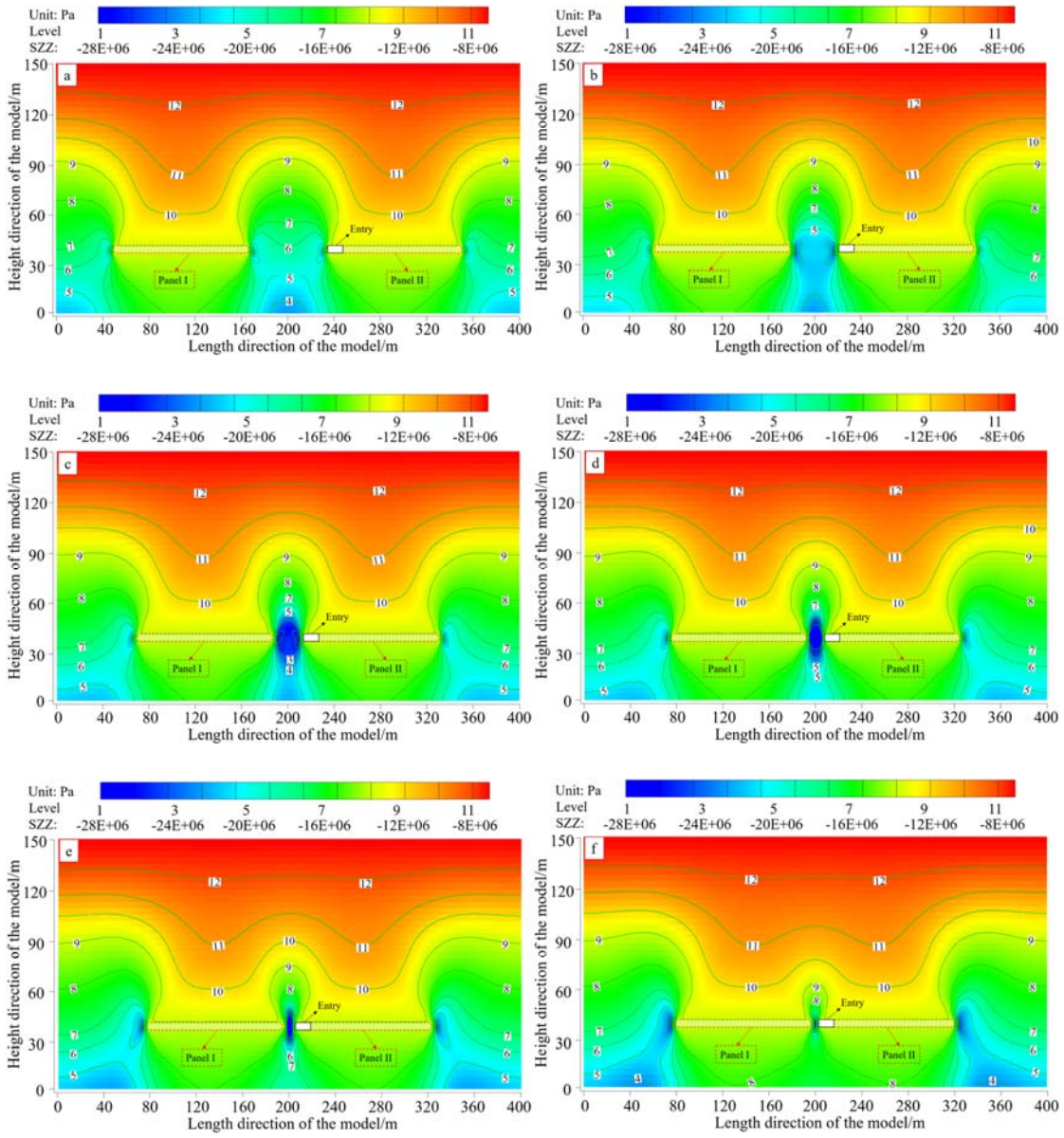

Figure 3. Evolution laws of the vertical stress on the entry wall. (**a**) The pillar width was 80 m. (**b**) The pillar width was 50 m. (**c**) The pillar width was 30 m. (**d**) The pillar width was 15 m. (**e**) The pillar width was 8 m. (**f**) The pillar width was 5 m.

2.2. *Experimental Analysis of the Entry Wall Stability*

2.2.1. Model Description at the Laboratory

According to rock damage theory, high stresses on the entry wall tend to produce more mining-induced fractures [23–25]. The degree of damage differs as the pillar width changes. Simulation results indicated that when the pillar was wide, the stress peaks were distributed at the sides. In this case, most fractures were distributed at the sides, and the central zone remained almost undamaged. Therefore, the central cubic zone was restricted in the horizontal direction and could be simplified to be laterally confined, as shown in Figure 4a.

In contrast, when the entry wall was narrow, the global stress was large, thus causing more voids and mining-induced fractures. In this case, the horizontal limit was weakened, and the lateral load accordingly reduced, as shown in Figure 4b,c. Combining these results with the practical situation on

site, we used cubic coal units confined with different amounts of lateral pressure to simply show the failure behaviors of the entry wall with different widths. This type of simplification has also been used by other researchers [26–28].

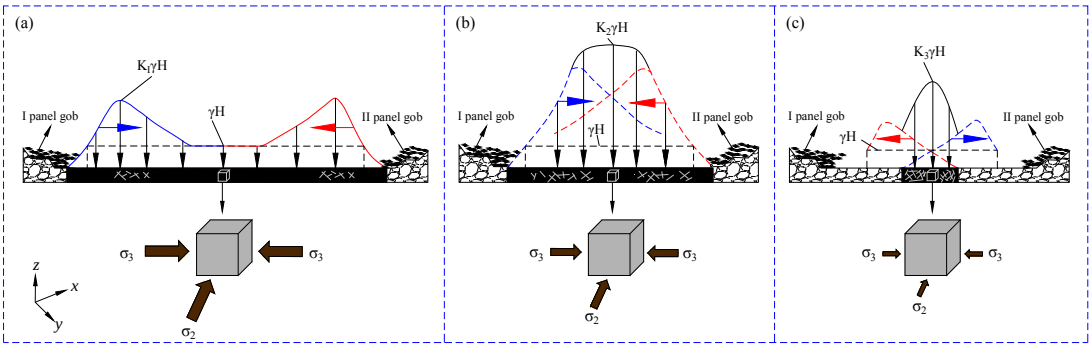

Figure 4. Model simplification at the laboratory. (**a**) A wide coal pillar. (**b**) A medium wide coal pillar. (**c**) A narrow coal pillar.

2.2.2. Methodology

The natural coal obtained on site was processed into cubic coal samples with a side length of 110 mm. Three intact samples were selected to investigate the pillar failure behaviors. The average density of the samples was 1.25 g/cm^3. These samples were tested in a true triaxial test unit, as shown in Figure 5. This equipment is mainly composed of a loading system, a pressure pump, a data collection system and a triaxial cell. These specimens were first put into a metal box to ensure stability and then installed in the triaxial cell. The equipment can accomplish automatic self-compensation of the pressure and control the confining pressure by utilizing a rock servo controlling rheological testing machine. This equipment can conduct the uniaxial compression test, the triaxial conventional compression test and the cyclic loading test, etc. During the test, the experimental data of the stress-strain curve can be recorded by the data acquisition system utilizing the corresponding sensors.

Figure 5. Test equipment at the laboratory.

Based on the crustal stress of the test site, these samples were confined with different lateral pressures to simulate different sized pillars, as described in Table 2. Because the strike length of the pillar is much larger than the width, thus we assume that the lateral pressures in the x direction are all the same (6.0 MPa). The first sample (S1) was confined with 2.0 MPa in the y direction to simulate a wide coal pillar. The second sample (S2) was confined with 1.0 MPa in the y direction to simulate

a medium sized coal pillar, and the third sample (S3) was confined with 0.5 MPa in the y direction to simulate a narrow coal pillar. First, a very small force was applied on the surface of the cubic samples at a rate of 0.5 kN/s. Subsequently, σ_x and σ_y were increased to the predetermined confining stresses, as listed in the Table 2. Finally, the samples were loaded at a stable rate of 0.004 mm/s in the z direction until the maximum displacement limitations were reached.

Table 2. Confining stresses loaded on the samples.

Sample	σ_z (Sample Faces)	σ_x (Sample Faces)	σ_2 (MPa)	σ_y (Sample Faces)	σ_3 (MPa)
S1	A & C	(E & F)	6.0	(B & D)	2.0
S2	A & C	(E & F)	6.0	(B & D)	1.0
S3	A & C	(E & F)	6.0	(B & D)	0.5

2.2.3. Test Results

Figure 6 shows the damage states of each sample after testing. It is obvious that when the σ_y was 2.0 MPa, the six faces of the S1 sample almost remained intact. There were only some micro-pores or micro-fractures distributed on the surfaces, indicating that the central zone of a wide pillar is less likely to be damaged. As the pillar width decreased, the confining stress also decreased. As seen from the damage state of S2 sample, two great fractures and many pores were generated on the surfaces. Furthermore, when the σ_y decreased to 0.5 MPa, the sample was crushed into blocks. The damage morphologies of the S1, S2 and S3 samples showed that as the confining stress decreased, the degree of damage of the samples became more serious.

Figure 7 shows the stress-strain curves during the test. The critical failure stresses of S1, S2 and S3 were 35.397 MPa, 23.379 MPa and 16.591 MPa, respectively. As the confining stress decreased, the peak stress decreased as well. From the post-peak behavior of the curves, we can see that when the confining stress is large, the change of the loading stress is gentler, indicating that a strong lateral restriction caused the wide coal pillar to be more stable.

The damage morphologies and stress-strain curves showed that when the pillar is wide, it would be favorable to avoiding entry instability problems. However, oversize pillars cause a serious waste of resources. Although mining with narrow pillars can save more resources, high stress concentrations and less lateral restrictions caused the entry wall to be more unstable. Hence, mining with coal pillars always involves a tradeoff between economy and safety.

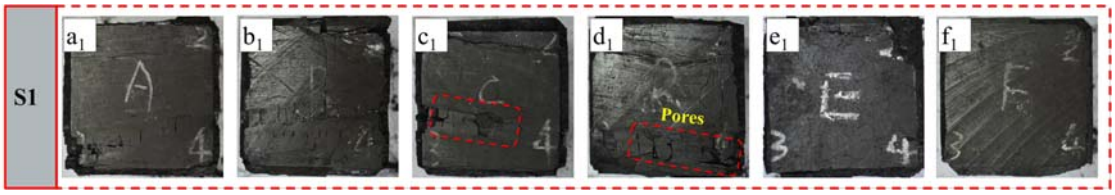

(**a**)

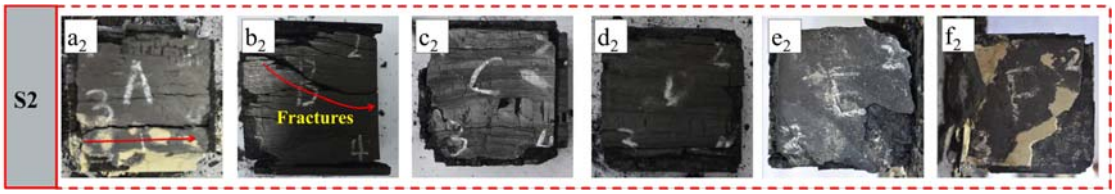

(**b**)

Figure 6. *Cont.*

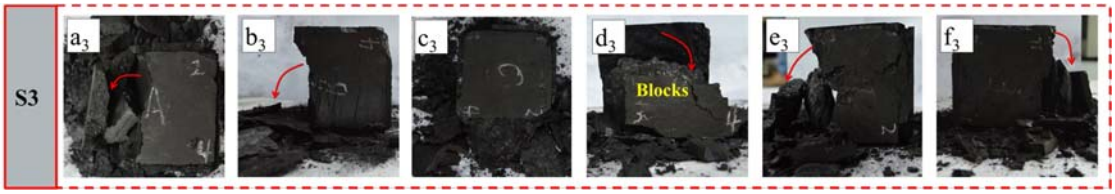

(**c**)

Figure 6. Damage states of the samples under different confining pressures. (**a**) Six faces of S1 sample. (**b**) Six faces of S2 sample. (**c**) Six faces of S3 sample.

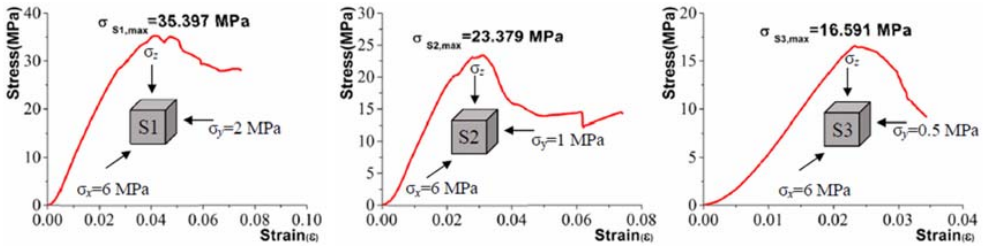

Figure 7. Z-direction stress-strain curves under different confining pressures. (**a**) S1 sample. (**b**) S2 sample. (**c**) S3 sample.

2.3. Theoretically Analysis of the Coal Pillar Stability

Numerical simulation indicated that entry stability was highly related to its surrounding stresses. As the pillar width decreased, the overall vertical stress acting on the coal pillar increased. When the pillar was too narrow to bear the concentrated stress, the entry wall was damaged. The laboratory test also showed that as the pillar width decreased (or confining pressure decreased), the coal body tended to be more unstable. Hence, we can understand that the width of the coal pillar is an important factor that affects the entry stability. In this section, the entry wall stability with regard to pillar width was theoretically investigated in three frequently used mining patterns, i.e., wide coal pillar mining, narrow coal pillar mining and non-pillar mining by filling artificial materials.

2.3.1. Wide Coal Pillar Mining

In the wide coal pillar mining, disturbances from the current mining panel have little influence on the next mining panel. When the current mining panel is working, the tail entry or head entry for the next mining panel can be tunneled at the same time, as shown in Figure 8. This type of mining pattern is especially suitable for the condition where many panels must be mined simultaneously.

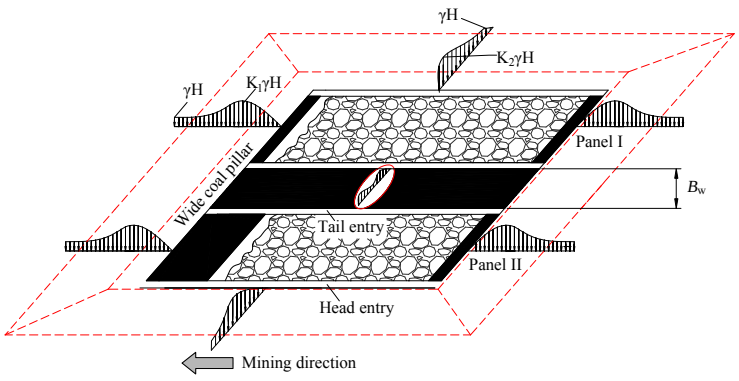

Figure 8. Plane layout of the wide coal pillar mining pattern.

When the pillar is wide, the coal pillar can be divided into four zones, i.e., fractured zone (I and I'), plastic zone (II and II'), elastic zone (III and III') and original stress zone (IV and IV'), along the pillar width direction, as shown in Figure 9. In fractured and plastic zones, the side abutment pressure can be expressed as [29]:

$$\sigma_1 = N_0 e^{\frac{2fx}{m}} \left(\frac{1+\sin\varphi}{1-\sin\varphi}\right), \tag{1}$$

where N_0 is the self-bearing capacity of the coal pillar; m is the mining height; f is the friction coefficient between roof rock and coal seam; x is the distance from the entry rib; φ is the internal friction angle of the coal.

The pressure at the elastic zone can be expressed as:

$$\sigma_2 = \left[1 + K_0 \frac{1}{e^{b(x-x_0)}}\right] \gamma H, \tag{2}$$

where H and γ are the thickness and unit weight of the overburden; x_0 is the range sum of fractured and plastic zones; K_0 and b are constant coefficients reflecting the coal and rock strength.

The pressure at the original stress zone can be written as:

$$\sigma_3 = \gamma H. \tag{3}$$

In this kind of mining pattern, the mining influence of panel I has little influence on the mining of panel I, and there is no pressure superposition on the coal pillar ($d \geq 0$). Thus, the maximum pressure on the coal pillar ($K_{I,II}\gamma H$) is only induced by one mining panel, and the pillar is relatively stable. This agrees with the numerical simulation and laboratory test results.

The design width of the wide coal pillar in this mining pattern can be written as [30]:

$$B_w \geq x_{w1} + x_{w2} + L_w, \tag{4}$$

where B_w is the design width of the pillar; x_{w1} and x_{w2} are the widths of the plastic deformation zone caused by the current and next working panels (panels I and II), respectively, and can be expressed using Equation (5); and L_w is the width of the kernel elastic zone (about two times of the mining height).

$$x_{w1,w2} = \frac{m\lambda}{2tg\varphi} \ln\left[\frac{K_{I,II}\gamma H + \frac{C}{tg\varphi}}{\frac{C}{tg\varphi} + \sigma_c}\right] + \frac{m}{2tg\varphi}\left[\ln\left(1 + \frac{K_{I,II}\gamma H}{C} tg\varphi\right)^{\lambda} + tg^2\varphi\right], \tag{5}$$

where λ is the side pressure coefficient; C is the internal friction angle of the coal; σ_c is the uniaxial compressive strength of the coal pillar; $K_{I,II}$ is the stress concentration factor induced by coal face mining.

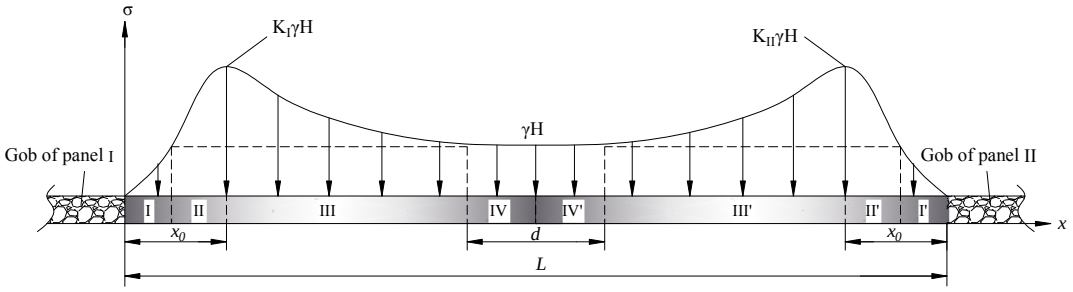

Figure 9. Stress distributions in a wide coal pillar mining pattern.

Generally, stabilities of the entry in a wide coal pillar mining pattern can be well guaranteed. However, oversize pillars usually cause large amounts of waste, accounting for approximately

10%~30% of the total coal production. In addition, each mining panel requires two entries that are mainly used for transportation and ventilation, which also increases construction cost and labor.

2.3.2. Narrow Coal Pillar Mining

The narrow coal pillar mining pattern is also known as gob-side entry driving [31–33]. The recovery ratio of this type of mining pattern is much larger than that of the wide coal pillar mining pattern, as shown in Figure 10.

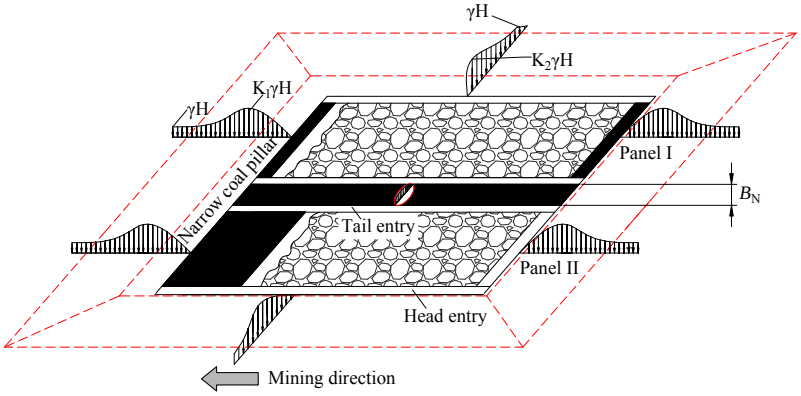

Figure 10. Plane layout of the narrow coal pillar mining pattern.

However, when the pillar is narrow, the side abutment pressures induced by two adjacent mining panels couple with each other, which causes the integral pressure to be larger than that of a wide coal pillar. In this kind mining pattern, there is no original stress zone, as shown in Figure 11. The coupled pressure on the coal pillar can be written as:

$$\sigma_3 = \left[1 + K_0 \frac{1}{e^{b(L-x)}}\right] \gamma H + N_0 e^{\frac{2fx}{m}} \left(\frac{1+\sin\varphi}{1-\sin\varphi}\right), \quad (6)$$

where L is the width of the coal pillar.

As seen from Equation (6), as the width of the coal pillar decreases, the integral pressure increases accordingly, owing to the stress superposition effects. When the stress state of the coal meets the failure criterion, the pillar will be damaged or crushed. The above theoretical model can well explain the numerical simulation and laboratory test results.

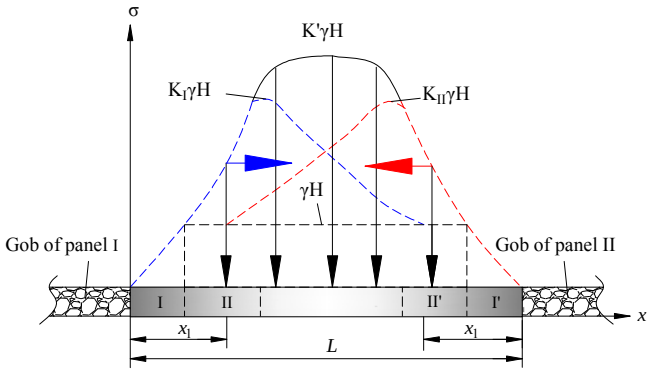

Figure 11. Stress distributions in a narrow coal pillar mining pattern.

The size of the pillar is difficult to be accurately determined for a narrow coal pillar mining pattern. If the width of the pillar is irrational, the mining-induced fractures in the pillar may lead to air leakage and spontaneous combustion. In addition, the entry for the next mining panel is near the peak

position of the side abutment pressure in most cases, which may cause strong strata movements and large deformations. The width of the coal pillar for the NCPM pattern can be expressed by [34,35]:

$$B_{\mathrm{N}} \geq X_1 + X_2 + X_3, \tag{7}$$

where X_1 is the width of the mining-induced plastic area in the NCPM and can be given by

$$X_1 = \frac{m\lambda}{2tg\varphi} \ln\left[\frac{K\gamma H + \frac{C}{tg\varphi}}{\frac{C}{tg\varphi} + \sigma_c}\right], \tag{8}$$

X_2 is the effective anchorage length of the bolt (cable); X_3 is the additional safety length considering pillar stabilities, empirically approximately 30%~50% of $(X_1 + X_2)$; and K is the stress concentration factor.

2.3.3. Non-pillar Mining

In development since the early 1950s, gob-side entry retaining is still one of the most commonly used techniques in non-pillar mining by filling artificial materials. In this technique, the former entry is artificially retained for the next mining panel by filling paste-like backfill material, high-water packing material and other artificial materials, as shown in Figure 12. The key technique of this mining pattern is that the narrow coal pillar is further replaced by the filling materials. However, the stress distribution on the artificial filing body is similar with that on a narrow coal pillar. The design width of the filling body can be written as [36]:

$$B_{\mathrm{F}} \geq \frac{kF_s}{\sigma'}, \tag{9}$$

where F_s is the roof pressure that acts on the filling body; σ' is the average compressive strength of the filling body, and k is the safety factor, approximately 1.1~1.2.

The application of this technique can reduce entry drivage ratios and increase coal recovery rates. However, the high stress concentration on the filling body and huge material waste problems are always a concern. If this type of mining pattern were used in a thick coal seam, the above problems would be more serious. Hence, it is imperative to find a more effective and economical method to improve entry stability and mining sustainability.

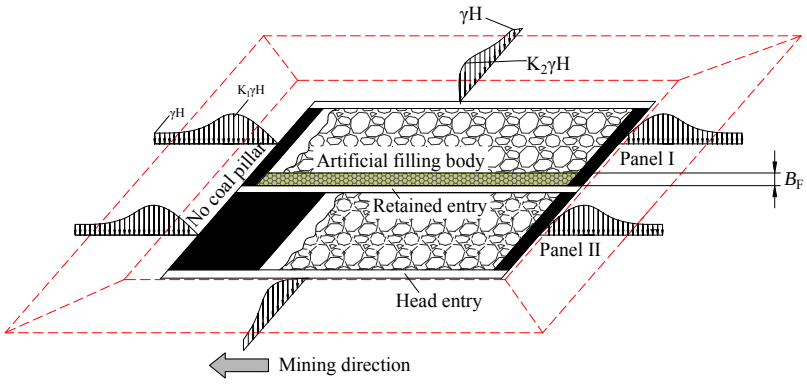

Figure 12. Plane layout of the non-pillar mining pattern.

3. Optimization of the Entry Stability in Longwall Mining

Numerical simulation showed that the coal pillar was always a stress-concentrated area in conventional longwall mining. Stress transmission induced by panel mining was the main reason accounting for instability of the entry walls. Laboratory tests indicated that a wide coal pillar was favorable for entry stabilities, but substantial waste of coal resources was a major concern. Although mining with narrow pillars can save more resources, the entry in this mining pattern

tended to be more unstable. Therefore, it can be concluded that coal pillar is one of the vulnerable entry surroundings where instability occurs. In the past few decades, non-pillar mining by filling artificial materials has been tested in many mines. However, the filling body is also a stress-concentrated area just as is the narrow coal pillar [37–39]. Additionally, excessive consumption of filling materials also sets limits on the popularity of this kind of mining pattern [40,41].

In longwall mining, roof caving is a complex dynamic process involving rock fracturing, disintegration and stress redistribution. Because movements of the entry and gob roof are always associated in the conventional mining patterns, the stress transmission from the gob roof is a main cause for stress concentration. Considering this, an innovative approach to improve entry stability by canceling the coal pillar and interrupting the stress transmission was proposed.

3.1. Directional Roof Fracturing (DRF) Technique

Before mining, the entry and gob roof compose the entire plate structure. After mining, the gob roof gradually caves due to the roof weighting. The movement of the gob roof inevitably imposes a pulling force on the entry roof, thus causing deformations in the entry roof. If the pulling force were reduced or prevented, the stress condition of the entry would be alleviated. Considering this, a stress optimization method by fracturing the roof was proposed, as shown in Figure 13. Unlike the none pillar mining by filling artificial materials, the entry in this method is retained utilizing the bulking roof rocks. After the roof is fractured, the stress transferring from the gob roof is disrupted. In this way, the coal pillar is entirely removed, and the pressure on the entry roof is correspondingly reduced. Additionally, the gob roof caves into loose gangues that bear the whole overburden. Because the bearing range of the loose gangue body is much larger than that of the coal pillar or artificial filling body, the stress concentration would be alleviated after adopting the technique.

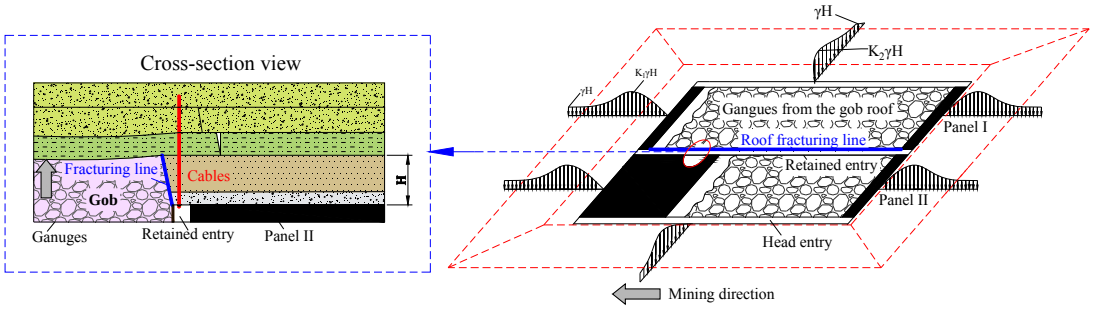

Figure 13. Principle of the mining pattern using the directional roof fracturing (DRF) technique.

Presently, blasting is primarily used to conduct roof fracturing in the field. To reduce disturbances on the entry roof, a directional roof fracturing (DRF) technique is proposed. In this technique, the blasting energy is actively controlled using an energy binding tube. The detonation generates high-speed, high-temperature and high-pressure gases that intensively act in the predetermined direction, as shown in Figure 14. Practice indicated that the DRF technique could not only protect the entry roof from blasting disturbances, but also be favorable for rock bulking.

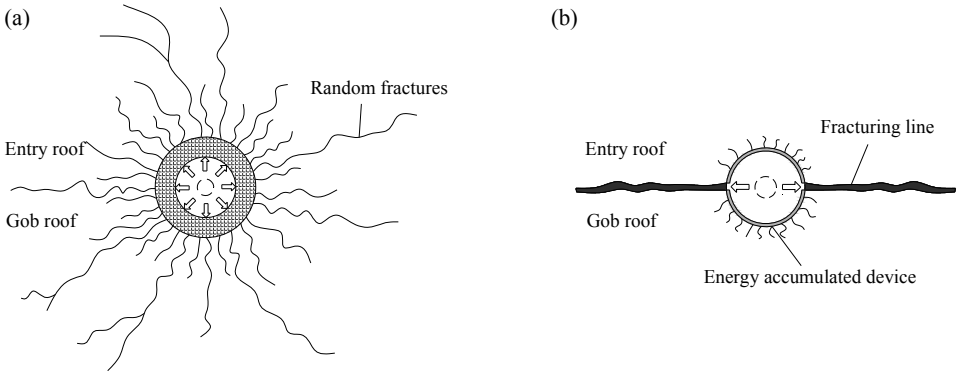

Figure 14. Active control of the crack propagation using the DRF technique. (**a**) Conventional blasting method. The blasting-induced cracks propagate in random directions in which case the entry roof might be damaged. (**b**) Directional blasting method. The blasting-induced cracks propagate in the predetermined direction in which case the entry roof can be well protected.

3.2. Stability Analysis of the Entry Using the Directional Roof Fracturing (DRF) Technique

3.2.1. Numerical Simulation

(1) Modeling scheme

Because the finite difference method is based on continuum mechanics, there are limitations in simulating roof caving problems. In contrast, the discrete element method (DEM) is a dynamic numerical method. The blocks or elements in the DEM modeling can shift, rotate or even separate from the main model. Therefore, the DEM is more applicable in simulating discontinuous and large deformation problems [42,43].

In this study, the DEM was used to explore entry stabilities under different mining conditions. The boundary conditions and mechanical parameters of the DEM model were same as those in the preceding FDM model. Three modeling schemes were compared in the simulation, as presented in Figure 15. The narrow pillar mining pattern with a 5-m coal pillar, which is commonly used in many mines, was first simulated. Subsequently, stabilities of the entry in the non-pillar mining using the DRF technique were studied. To highlight the effects of the DRF technique, a non-pillar mining condition without using the DRF technique has also been simulated. It is generally known that roof deformation is an important factor describing entry stabilities. To quantify the stabilities of the entry in different mining conditions, monitoring points were respectively established at the middle of the entry roof.

(2) Stability analysis of the entry in the simulation

Figure 15 shows the structural morphologies of the entry and vertical displacement of the roof after mining. In the narrow coal pillar mining pattern, there was a long hanging roof structure above the entry wall (pillar), which easily caused stress concentrations and deformations. When the strength of the pillar cannot bear the overburden, an instability phenomenon would occur. As seen from Figure 15a, the entry wall has obviously deformed under the above heavy loads. The maximum sagging value of the entry roof was approximately 835 mm in the first scheme.

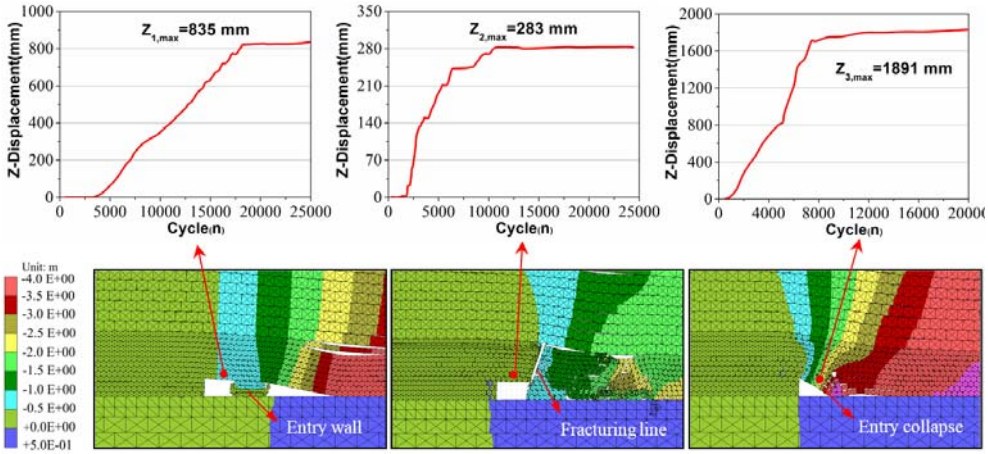

(**a**) (**b**) (**c**)

Figure 15. Structural morphologies and displacement variation under different simulation conditions. (**a**) The narrow coal pillar mining condition; (**b**) Non-pillar mining using the DRF technique; (**c**) Non-pillar mining without using the DRF technique.

Compared with the narrow coal pillar mining pattern, the roof subsidence decreased about 66% to 283 mm after adopting the DRF technique. After fracturing, the motion state of the entry and gob roof became less associated. The gob roof caved into gangues along the fracturing line. The bulking gangues effectively supported the main roof, which helped decrease the amount of roof sagging.

Furthermore, if the roof was not fractured, the entry roof collapsed together with the gob roof, as shown in Figure 15c. The amount of roof sagging at the monitoring point was approximately 1891 mm in the last scheme. From the simulation results, especially the second and last schemes, we can understand that the roof fracturing exerted a significant influence on the movement of the surrounding rocks. The entry roof was not only in a low stress environment but also deformed less after taking the new technique. In a certain geological condition, entry stabilities using the DRF technique was better than that using the conventional mining method.

3.2.2. Field Test

(1) Test Process

Roof fracturing height is one of the key parameters in the DRF technique. The fracturing height should be sufficient to fill the mining room with bulking gangues [44]. The fracturing height can be calculated by:

$$H = \frac{h_c - h_s - h_h}{k - 1}, \tag{10}$$

where h_c is the mining height; h_s is the amount of floor sagging; h_h is the amount of bottom bulging; and k is the bulking coefficient of the gob roof.

Based on the actual condition of the S1201 mining panel in the Ningtiaota coal mine, the bulking coefficient of the gob roof is approximately 1.39. The average amounts of bottom bulging and floor sagging were 310 mm and 360 mm, respectively. Considering the theoretical result and field condition, the fracturing height was finally determined to be 9.0 m.

Test processes of the DRF technique were as follows (see Figure 16).

(i) Drill fracturing holes. The fracturing holes were marked on the roof in advance. The hole diameter and spacing were 46 mm and 600 mm, respectively. To reduce disturbances from the gob roof caving, the fracturing angle must be consistent, tilting ten degrees towards the mined-out area.

(ii) Install energy binding tubes. First, the energy binding tubes were charged with emulsified blasting powders outside the fracturing holes. Subsequently, the tubes together with the powders were put into the holes. Note that the energy-accumulated direction must be same, in which case a continuous fracturing line could be formed.

(iii) Perform roof fracturing. After blasting, the cracks formed a fracturing line on the surface of the entry roof. As the mining panel advanced, the gob roof gradually caved along the fracturing line, and the caved gangues formed a special entry wall (gangue rib).

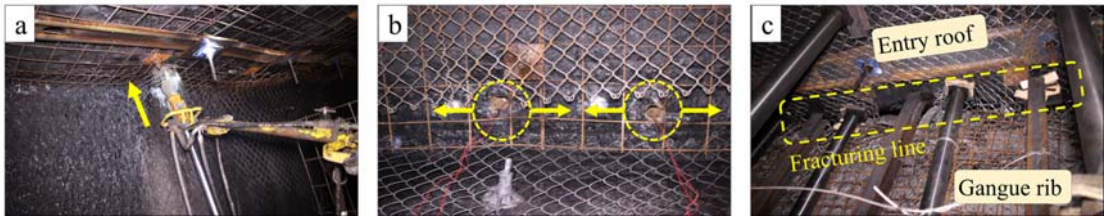

Figure 16. Test processes of the DRF technique. (**a**) Drilling fracturing holes; (**b**) Charging with energy binding tubes; (**c**) Roof fracturing effects.

(2) Stability Analysis of the Entry in the Field

To explore the influence of the DRF technique in the field, a KJ216 pressure monitoring apparatus was installed on the face-end support beside the entry, as shown in Figure 17. This apparatus could continuously and automatically record the roof pressure during the mining process. The monitoring distances of the non-fracturing and fracturing condition were both 150 m.

Figure 18 shows the variation of the roof pressure before and after adopting the DRF technique. It can be seen that the maximum roof pressure was 19.5 MPa after roof fracturing, 8.7 MPa smaller than that in the non-fracturing condition. The average roof pressure decreased by appropriately 60% to 7.1 MPa after adopting the new technique. Field monitoring indicated that the DRF technique could effectively optimize the stress condition of the entry. This would also be favorable to stabilities and safeties of the entry in follow-up maintenance.

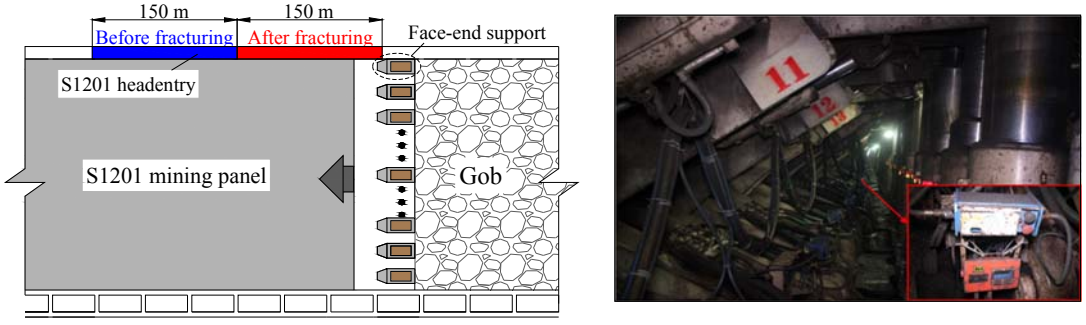

Figure 17. Sketch of the field monitoring and apparatus. (**a**) Monitoring position and scope;(**b**) KJ216 monitoring apparatus for roof pressure.

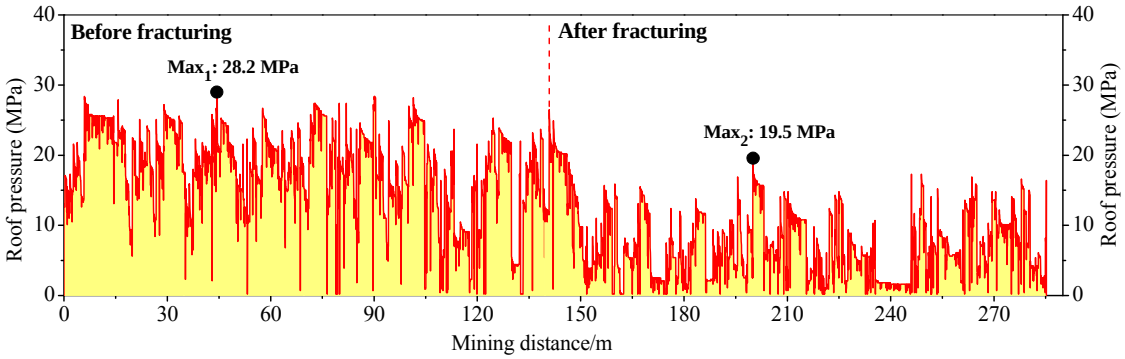

Figure 18. Variation of the roof pressure before and after adopting the DRF technique.

Figure 19 shows the final entry retaining photos after adopting the DRF technique. The gob roof collapsed into gangues along the fracturing line. The caved gangues replaced the coal pillar or artificial filling body and became another entry rib. During caving and compaction of the gangues, gangue prevention structures and metal nets were used to prevent the gangues from extending out into the entry, as illustrated in Figure 19a. Once the gangues and main roof had been stabilized, air leakage prevention materials were sprayed on the surface of the gangue rib, as shown in Figure 19b. The mean sagging amount of the entry roof was approximately 258 mm. The cross-section of the retained entry could fully meet requirements of the next mining panel. The field test revealed that the DRF technique could effectively improve stabilities of the entry.

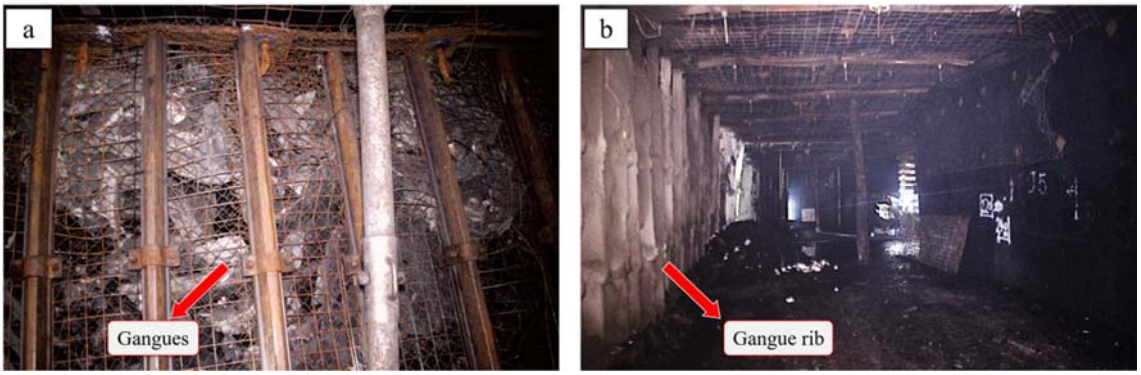

Figure 19. Entry retaining effects after adopting the new technique. (**a**) Roof caving effects; (**b**) Entry retaining effects.

4. Conclusions

In China, coal provides most of the energy for the development of economy and industrialization. Mining depth is gradually increasing due to limited coal resources in shallow depth. Exploiting the valuable coal resources efficiently and safely is meaningful to the sustainable development of resources and energy, as well as the economy and society. In this paper, the stability of the entry is selected as the research target. The main conclusions in this paper are listed as follows.

(1) Simulations of different mining patterns showed that mining activities could cause stress concentrations on the entry wall. When the width of the entry wall was more than 30 m, there were two stress peaks distributed on the sides. As the width decreased, the stress peaks moved closer to each other and gradually merged into one. During this process, the vertical stresses caused by two mining panels, coupled with each other, and the integrated stress gradually increased. However, when the width was less than 10 m, the coupling stress decreased unexpectedly.

(2) Entry wall stabilities were simply explored using representative coal units at the laboratory. True triaxial tests showed that, as the confining stress decreased, the critical buckling load decreased, and the degree of damage became more serious. The testing results implied that a wide pillar was more stable than a narrow one. Nevertheless, the serious waste of resources was a considerable concern for mining with wide coal pillars. Hence, mining with coal pillars always involves a tradeoff between economy and safety.

(3) Considering the existing problems of longwall mining with coal pillars, an innovative approach to improve entry stabilities by optimizing the stress distributions was introduced. In this approach, the geometry of the entry and gob roofs is actively controlled by roof fracturing along with support, thus reducing stress in the retained entry. Additionally, bulking characteristics of the caving gangues at the gob area are efficiently used, and no extra man-made filling material is therefore needed, which makes this approach more flexible and cost effective compared with other previous approaches. Numerical modeling showed that the DRF technique could prevent stress transfer from the gob roof to entry roof, thus causing the entry to be more stable. The deformation of the entry roof decreased by approximately 66% compared with that using the conventional mining method. Field tests indicated that the average roof pressure decreased by approximately 60% after adopting the new technique. Together, these results suggested that the DRF technique could not only avoid resource waste but also be favorable to improving entry stabilities.

Acknowledgments: This work is supported by the National Natural Science Foundation of China (No. 51704298, No. 51674265) and the State Key Research Development Program of China (No. 2016YFC0600900), which are gratefully acknowledged.

Author Contributions: Manchao He and Yubing Gao proposed the new technique and conceived the experiments; Yubing Gao and Xingyu Zhang performed the numerical simulation and field tests; Yubing Gao and Dongqiao Liu performed the laboratory experiments; Yubing Gao analyzed the data and wrote the paper.

Conflicts of Interest: The authors declare no conflict of interest.

References

1. Milici, R.C.; Flores, R.M.; Stricker, G.D. Coal resources, reserves and peak coal production in the United States. *Int. J. Coal Geol.* **2013**, *113*, 109–115. [CrossRef]
2. Lechner, A.M.; Kassulke, O.; Unger, C. Spatial assessment of open cut coal mining progressive rehabilitation to support the monitoring of rehabilitation liabilities. *Resour. Policy* **2016**, *50*, 234–243. [CrossRef]
3. Shabanimashcool, M.; Li, C.C. A numerical study of stress changes in barrier pillars and a border area in a longwall coal mine. *Int. J. Coal Geol.* **2013**, *106*, 39–47. [CrossRef]
4. Suchowerska, A.M.; Merifield, R.S.; Carter, J.P. Vertical stress changes in multi-seam mining under supercritical longwall panels. *Int. J. Rock Mech. Min. Sci.* **2013**, *61*, 306–320. [CrossRef]
5. Basarir, H.; Ferid Oge, I.; Aydin, O. Prediction of the stresses around main and tail gates during top coal caving by 3D numerical analysis. *Int. J. Rock Mech. Min. Sci.* **2015**, *76*, 88–97. [CrossRef]
6. Su, D.W. Effects of longwall-induced stress and deformation on the stability and mechanical integrity of shale gas wells drilled through a longwall abutment pillar. *Int. J. Min. Sci. Technol.* **2017**, *27*, 115–120. [CrossRef]
7. Gao, Y.; Liu, S.; Lyu, B.; Li, K. Mechanism study of floor water inrush around mining field based on micro-crack extension. *J. Min. Saf. Eng.* **2016**, *33*, 624–629.
8. Cheng, G.; Ma, T.; Tang, C.; Liu, H.; Wang, S. A zoning model for coal mining—Induced strata movement based on microseismic monitoring. *Int. J. Rock Mech. Min. Sci.* **2017**, *94*, 123–138. [CrossRef]
9. Tu, S.; Wang, F.; Dou, F.; Yuan, Y.; Lu, Y. Fully mechanized top-coal caving: Underground stress at gate ways under barrier pillars of an upper coal seam. *J. China Univ. Min. Technol.* **2010**, *39*, 1–5.
10. Kang, H.; Wu, Y.; Gao, F. Deformation characteristics and reinforcement technology for entry subjected to mining-induced stresses. *J. Rock Mech. Geotech. Eng.* **2011**, *3*, 207–219. [CrossRef]
11. Wei, G. Study on the width of the non-elastic zone in inclined coal pillar for strip mining. *Int. J. Rock Mech. Min. Sci.* **2014**, *72*, 304–310. [CrossRef]

12. Wang, S.; Hao, S.; Chen, Y.; Bai, J.; Wang, X.; Xu, Y. Numerical investigation of coal pillar failure under simultaneous static and dynamic loading. *Int. J. Rock Mech. Min. Sci.* **2016**, *84*, 59–68. [CrossRef]
13. Reed, G.; Mctyer, K.; Frith, R. An assessment of coal pillar system stability criteria based on a mechanistic evaluation of the interaction between coal pillars and the overburden. *Int. J. Min. Sci. Technol.* **2017**, *27*, 9–15. [CrossRef]
14. Wattimena, R.K.; Kramadibrata, S.; Sidi, I.D.; Azizi, M.A. Developing coal pillar stability chart using logistic regression. *Int. J. Rock Mech. Min. Sci.* **2013**, *58*, 55–60. [CrossRef]
15. Das, A.J.; Mandal, P.K.; Ghosh, C.N.; Sinha, A. Extraction of locked-up coal by strengthening of rib pillars with FRP-A comparative study through numerical modelling. *Int. J. Min. Sci. Technol.* **2017**, *27*, 261–267. [CrossRef]
16. Yang, J.; Yu, S.; Tao, Z.; Sun, X.; Wang, D. On the deformation and failure characteristics of the tertiary soft rock entry and coupling control measures. *J. Min. Saf. Eng.* **2014**, *31*, 373–378.
17. He, M.; Gao, Y.; Yang, J.; Guo, Z.; Wang, E.; Wang, Y. An energy-gathered roof cutting technique in no-pillar mining and its impact on stress variation in surrounding rocks. *Chin. J. Rock Mech. Eng.* **2017**, *36*, 1314–1325.
18. Zhang, N.; Yuan, L.; Han, C.; Xue, J.; Kan, J. Stability and deformation of surrounding rock in pillarless gob-side entry retaining. *Saf. Sci.* **2012**, *50*, 593–599. [CrossRef]
19. Islavath, S.R.; Deb, D.; Kumar, H. Numerical analysis of a longwall mining cycle and development of a composite longwall index. *Int. J. Rock Mech. Min. Sci.* **2016**, *89*, 43–54. [CrossRef]
20. Shabanimashcool, M.; Li, C.C. Numerical modelling of longwall mining and stability analysis of the gates in a coal mine. *Int. J. Rock Mech. Min. Sci.* **2012**, *51*, 24–34. [CrossRef]
21. Cheng, Y.; Wang, J.; Xie, G.; Wei, W. Three-dimensional analysis of coal barrier pillars in tailgate area adjacent to the fully mechanized top caving mining face. *Int. J. Rock Mech. Min. Sci.* **2010**, *47*, 1372–1383. [CrossRef]
22. Cai, M.; He, M.; Liu, D. *Rock Mechanics and Engineering*; Science Press: Beijing, China, 2013; pp. 32–38.
23. Wang, G.; Wu, M.; Wang, R.; Xu, H.; Song, X. Height of the mining-induced fractured zone above a coal face. *Eng. Geol.* **2017**, *216*, 140–152. [CrossRef]
24. Jing, Y.; Armstrong, R.T.; Mostaghimi, P. Rough-walled discrete fracture network modelling for coal characterisation. *Fuel* **2017**, *191*, 442–453. [CrossRef]
25. Su, F.; Itakura, K.; Deguchi, G.; Ohga, K. Monitoring of coal fracturing in underground coal gasification by acoustic emission techniques. *Appl. Energy* **2017**, *189*, 142–156. [CrossRef]
26. Huang, Z.; Dai, X.; Dong, L. Buckling failures of reserved thin pillars under the combined action of in-plane and lateral hydrostatic compressive forces. *Comput. Geotech.* **2017**, *87*, 128–138. [CrossRef]
27. Chen, S.; Guo, W.; Cheng, G.; Zhao, T. Research on creep supporting effect of deep strip pillar. *J. Min. Saf. Eng.* **2012**, *29*, 48–53.
28. Song, Y.; Yang, X. Evolution characteristics of deformation and energy fields during coal pillar instability. *J. Min. Saf. Eng.* **2013**, *30*, 822–827.
29. Gu, S.; Jiang, B.; Wang, C.; Li, N. Simulation research on overburden failure and lead abutment pressure distribution of fully-mechanized sublevel caving face. *Min. Res. Dev.* **2013**, *33*, 11–14.
30. Zhang, W.; Kong, X.; Kang, T.; Zhao, G. Research on reasonable size of large coal pillar between panels at mining face with soft surrounding rock. *Min. Res. Dev.* **2013**, *33*, 14–17.
31. Zhang, Y.; Wan, Z.; Li, F.; Zhou, C.; Zhang, B.; Guo, F.; Zhu, C. Stability of coal pillar in gob-side entry driving under unstable overlying strata and its coupling support control technique. *Int. J. Min. Sci. Technol.* **2013**, *23*, 193–199. [CrossRef]
32. Song, Z.; Cui, Z.; Xia, H.; Tang, J.; Wen, Z. The fundamental theoretical and engineering research on the green safe no coal pillar mining model by mainly using coal gangue backfill. *J. China Coal Soc.* **2010**, *35*, 705–710.
33. Hou, C.; Li, X. Stability principle of big and small structures of rock surrounding entry driven along goaf in fully mechanized top coal caving face. *J. China Coal Soc.* **2001**, *26*, 1–7.
34. Zhang, K.; Jiang, Y.; Zhang, Z.; Zhang, Y.; Pang, X.; Zeng, X. Determining the reasonable width of narrow pillar of entry in gob entry driving in the large pillar. *J. Min. Saf. Eng.* **2014**, *31*, 255–262.
35. Wang, D.; Li, S.; Wang, Q.; Li, W.; Wang, F.; Wang, H.; Peng, P.; Ruan, G. Experimental study of reasonable coal pillar width in fully mechanized top coal caving face of deep thick coal seam. *Chin. J. Rock Mech. Eng.* **2014**, *33*, 539–548.
36. Huang, Y.; Sun, H. Design of gob-side packing parameters for gateways maintained along the goaf. *J. China Coal Soc.* **1997**, *22*, 127–131.

37. Zhang, J.; Li, B.; Zhou, N.; Zhang, Q. Application of solid backfilling to reduce hard-roof caving and longwall coal face burst potential. *Int. J. Rock Mech. Min. Sci.* **2016**, *88*, 197–205. [CrossRef]
38. Zhang, Z.; Bai, J.; Chen, Y.; Yan, S. An innovative approach for gob-side entry retaining in highly gassy fully-mechanized longwall top-coal caving. *Int. J. Rock Mech. Min. Sci.* **2015**, *80*, 1–11. [CrossRef]
39. Zhang, G.; He, M.; Yu, X.; Huang, Z. Research on the technique of no-pillar mining with gob-side entry formed by advanced roof caving in the protective seam in Baijiao coal mine. *J. Min. Saf. Eng.* **2011**, *28*, 511–516.
40. Bu, T.; Feng, G.; Jia, K. Gateway side backfilling support technology of goaf side gateway in fully mechanized high cutting longwall mining face. *Coal Sci. Technol.* **2010**, *38*, 41–44.
41. Ma, L.; Zhang, D.; Wang, H.; Li, Y. Mining technique with preset packing body in entry for thick coal seam without coal pillars. *Chin. J. Rock Mech. Eng.* **2010**, *29*, 674–680.
42. Leclerc, W.; Haddad, H.; Guessasma, M. On the suitability of a Discrete Element Method to simulate cracks initiation and propagation in heterogeneous media. *Int. J. Solids Struct.* **2017**, *108*, 98–114. [CrossRef]
43. Gui, Y.L.; Zhao, Z.Y.; Kodikara, J.; Bui, H.H.; Yang, S.Q. Numerical modelling of laboratory soil desiccation cracking using UDEC with a mix-mode cohesive fracture model. *Eng. Geol.* **2016**, *202*, 14–23. [CrossRef]
44. Gao, Y.; Guo, Z.; Yang, J.; Wang, J.; Wang, Y. Steady analysis of gob-side entry retaining formed by roof fracturing and control techniques by optimizing mine pressure. *J. China Coal Soc.* **2017**, *42*, 1672–1681.